行政院國家科學委員會補助專題研究計畫成果報告

※※※※※※※※※※※※※※※※※※※※※※※※※
※ ※
※ **黏性流在移動座標上之分析**(II) ※
※ ※
※※※※※※※※※※※※※※※※※※※※※※※※※

計畫類別：□**個別型計畫**　　□**整合型計畫**
計畫編號：NSC　89－2611－E－002－001－
執行期間：　88 **年** 08 **月** 01 **日至** 89 **年** 07 **月** 31 **日**

計畫主持人：許文翰

本成果報告包括以下應繳交之附件：

□**赴國外出差或研習心得報告一份**
□**赴大陸地區出差或研習心得報告一份**
□**出席國際學術會議心得報告及發表之論文各一份**
□**國際合作研究計畫國外研究報告書一份**

執行單位：國立台灣大學造船及海洋工程學系所

中　華　民　國 90 **年** 02 **月** 18 **日**

有限元素方法分析在可變彈性體內之不可壓縮流

Finite element simulation of incompressible fluid flow in compliant elastic vessels

計畫編號：NSC 89-2611E-002-033
執行期限：88 年 8 月 1 日至 89 年 7 月 31 日
主持人：許文翰　　國立台灣大學造船及海洋工程學系所

一、中文摘要

本文係以有限元素方法分析在彈性體內之不可壓縮流。離散方法是建制在加權餘數及 semi-discretization 之架構上。由于物理域將隨時間而異，故網格移動的過程中必需保持空間守恆性。方法之驗證係透過具理論解之求解。所求得在時間上準確之解非常接近實解。此外，吾人亦透過于具彈性管中之流體計算，以驗證具動格點程式之正確性。

關鍵詞：有限元素方法、不可壓縮、移動網格、彈性

Abstract

We present in this paper finite element analysis of Navier-Stokes equations in a domain partly bounded by an elastic medium. The method of weighted residuals is used together with the semi-discretization approach to obtain the discrete equations. In this approach, where the physical domain is allowed to vary, care is taken to retain the space conservation law property in the transformation of equations between fixed and moving grids. The validity of this method has been tested against several problems which are amenable to analytic solutions. Time accurate results show favorable agreement with analytic solutions. Having verified the applicability of the finite element code to problems involving moving grids, we consider fluid flow in a vessel, where part of its boundary moves over time. Both rigid and elastic vessel walls are considered, with emphasis placed on the validation of the formulation developed within the moving-grid framework.

Keywords: finite element, incompressible,Navier-Stokes,moving grids, elastic

二、Introduction

Flows in a domain bounded by time-varying boundaries can be encountered when simulating internal combustion engine flows, surface-ship flows, and blood flows in compliant arteries. Considering that the physical boundary is a part of the solution procedures, it adds complexity to modeling the flow physics from the working equations. With the advent of faster computers and ever-improving numerical methods, it is now possible to tackle transient fluid flows in a time-varying elastic vessel. The problem of this type is hemodynamically important for understanding more about the unsteady flow separation and, thus, the early stage of atherosclerosis formation (Ku, Giddens, Zarins & Glagov 1985). This motivated us to perform computationally more complex flow-structure analyses on moving grids.

In the numerical simulation of unsteady flows, moving boundary problems have been considered by relatively few authors. Demirdizic & Peric (1990) provided some useful information and discussed ways to handle problems with moving boundaries. Solutions for this class of problems are best analyzed in non-Eulerian (moving) coordinates. In this way, we can derive the conservation equations for fluid flows in moving coordinates through transformation of variables. One can also derive working equations more straightforwardly in general moving coordinates based on the concept of the Lie derivative (Ogawa Satoru & Ishiguro

Tomiko (1987) and Schouten (1954)). The grid fitted to the body moves in time and is not fixed in space. For analyses conducted in moving grids, it is important to satisfy the space conservation law (SCL) (Trulio & Trigger 1961) for purposes of properly relating the change of the cell area to the coordinate frame velocity. Failure to satisfy the space conservation law will cause the mass to accumulate or diminish. Thomas and Lombard (1979) were among the first to address the necessity of applying this constraint equation simultaneously with other conservation equations. Demirdzic and Peric (1983) later provided computational evidence to justify the rational use of the SCL constraint condition when simulating problems on non-stationary grids. In the present study, we adopted the moving grid concept in the finite element analysis.

The remainder of this paper is organized as follows. In the next section, we derived working equations on moving grids and briefly outlined the finite element discretization method. We then provide analytical verification of our proposed scheme formulated in moving grids. We also provide equations which govern the motion of a linearly elastic, incompressible, isotropic solid vessel. In the following section, we present numerical simulation of incompressible fluid flow in a vessel which partly undergoes a large-amplitude oscillation. Finally, we offer some conclusion remarks.

三、Mathematical Model

The problem of present interest falls into the incompressible flow category. The equation governing a viscous fluid flow in grids fixed in space is as follows:

$$\circ\frac{\partial\overline{\Phi}}{\partial t}+\frac{\partial}{\partial x}\left(\circ u\overline{\Phi}\right)+\frac{1}{r^{\sim}}\frac{\partial}{\partial y}\left(r^{\sim}\circ v\overline{\Phi}\right)=\frac{\partial}{\partial x}\left(\kappa\frac{\partial\overline{\Phi}}{\partial x}\right)+\frac{1}{r^{\sim}}\frac{\partial}{\partial y}\left(\kappa\frac{\partial\overline{\Phi}}{\partial y}\right)+S \quad (1)$$

Provided that $\overline{\Phi}=1$ and $S=0$, the above equation denotes the continuity equation. For equations with $\overline{\Phi}=u$ or v, $S=-\nabla p$, they stand for the x- and y-momentum equations, respectively. The above equation generalizes the truly two-dimensional case when $\sim$ is assigned to be zero and the angle-independent equations in cylindrical coordinates when $\sim$ is assigned to be 1. For simplicity of presentation we consider the following equations written in x–y coordinates:

$$\frac{\partial u}{\partial x}+\frac{\partial v}{\partial y}=0, \quad (2)$$

$$\frac{\partial u}{\partial t}+u\frac{\partial u}{\partial x}+v\frac{\partial u}{\partial y}=-\frac{1}{\circ}\frac{\partial p}{\partial x}+\frac{\kappa}{\circ}\left(\frac{\partial^2 u}{\partial x^2}+\frac{\partial^2 u}{\partial y^2}\right) \quad (3)$$

$$\frac{\partial v}{\partial t}+u\frac{\partial v}{\partial x}+v\frac{\partial v}{\partial y}=-\frac{1}{\circ}\frac{\partial p}{\partial y}+\frac{\kappa}{\circ}\left(\frac{\partial^2 v}{\partial x^2}+\frac{\partial^2 v}{\partial y^2}\right) \quad (4)$$

The above primitive-variable formulation involves a velocity vector $\underline{u}=(u,v)$ and pressure p for a fluid with kinematic viscosity κ. The advantage of adopting equations (2-4) is that this primitive variable formulation accommodates closure initial and boundary conditions (Ladyzhenskaya 1969).

For the sake of accuracy, adaptation of grid lines to the flow is desirable when simulating a flow whose boundary varies with time. Under these circumstances, movement of grid lines warrants careful consideration when carrying out flux discretization. To describe the method, it is instructive to consider the following prototype equation:

$$\frac{\partial\alpha}{\partial t}+u\frac{\partial\alpha}{\partial x}+v\frac{\partial\alpha}{\partial y}-\frac{\kappa}{\circ}\left(\frac{\partial^2\alpha}{\partial x^2}+\frac{\partial^2\alpha}{\partial y^2}\right)=0. \quad (5)$$

We can now rewrite equation (5) in moving grids (ξ,η) at time t.

Based on the one-to-one transformation between coordinates (ξ,η) and the fixed ones $x=x(\xi,\eta,t)$, $y=y(\xi,\eta,t)$ the material derivative of α can, by definition, be expressed as

$$\left.\frac{D\alpha}{Dt}=\frac{\partial\alpha}{\partial t}\right|_{(\xi,\eta)}=\left.\frac{\partial\alpha}{\partial t}\right|_{(x,y)}+\left.\frac{\partial\alpha}{\partial x}\frac{\partial x}{\partial t}\right|_{(\xi,\eta)}+\left.\frac{\partial\alpha}{\partial y}\frac{\partial y}{\partial t}\right|_{(\xi,\eta)}. \quad (6)$$

Define the grid velocity vector $\underline{v}_g=(u_g, v_g)$,

where $u_g = \left.\frac{\partial x}{\partial t}\right|_{(\xi,\eta)}$ and $v_g = \left.\frac{\partial y}{\partial t}\right|_{(\xi,\eta)}$; we can rewrite equation (6) as

$$\left.\frac{\partial \phi}{\partial t}\right|_{(x,y)} = \left.\frac{\partial \phi}{\partial t}\right|_{(\xi,\eta)} - \nabla\phi \cdot \underline{v}_g \quad (7)$$

Substitution of equation (7) into equation (5) yields

$$\left.\frac{\partial \phi}{\partial t}\right|_{(\xi,\eta)} + (u-u_g)\phi_x + (v-v_g)\phi_y - \frac{\mu}{\rho}(\phi_{xx}+\phi_{yy}) = 0. \quad (8)$$

Thanks to the above theoretical basis, we can transform flow equations (2-4) in fixed grids into their moving coordinate counterparts:

$$u_x + v_y = 0, \quad (9)$$

$$u_t + (u-u_g)u_x + (v-v_g)u_y = -\frac{1}{\rho}p_x + \frac{\mu}{\rho}(u_{xx}+u_{yy}), \quad (10)$$

$$u_t + (u-u_g)u_x + (v-v_g)u_y = -\frac{1}{\rho}p_x + \frac{\mu}{\rho}(u_{xx}+u_{yy}). \quad (11)$$

The formulation of flow-structure interaction problem is followed by deriving a differential equation for a compliant material which is subjected to a finite deformation. To simplify the analysis, we consider a medium whose elastic properties are identical in all directions. The equations of equilibrium for a homogeneous isotropic elastic solid can be derived by invoking the D'Alembert principle and adding the body force $\overline{F}$ ($\equiv F_i$, i = 1, 2) to the inertia force, yielding

$$\tau_{ij,j} + F_i = \rho_w \ddot{d}_i. \quad (12)$$

In the above, $\ddot{d}_i$ denote $\frac{d^2 d_i}{dt^2}$, where $\underline{d}$ = (d_1, d_2) and ρ_w, are known as the displacement vector and the density of the vessel wall, respectively. To close the differential system for modeling wall motion, a stress-strain equation for the elastic medium is needed. For an elastic material, its stress is, in general, nonlinearly dependent on the strain. We consider here the following linearly elastic material prior to simulating the physically more realistic and computationally more difficult nonlinear elasticity equation. Under these circumstances, the stress tensor is linearly related to the strain tensor as follows:

$$\tau_{ij} = \lambda\delta_{ij}d_{k,k} + G(d_{i,j} + d_{j,i}) \quad (13)$$

The above constitutive equation involves the Lame's constants (or elastic constants), G and λ. These material constants are, as usual, written in terms of the Young's modulus E and Poisson ratio $\overline{\nu}$:

$$G = \frac{E}{2(1+\overline{\nu})}, \quad (14)$$

$$\lambda = \frac{\overline{\nu}E}{(1+\overline{\nu})(1-2\overline{\nu})}. \quad (15)$$

Substituting equation (13) into (12), one obtains the well-known Navier equations for a linearly elastic medium given below:

$$\rho_w\frac{d^2 d_1}{dt^2} - \frac{\partial}{\partial x}\left[(\lambda+2G)\frac{\partial d_1}{\partial x} + \lambda\frac{\partial d_2}{\partial y}\right] - \frac{\partial}{\partial y}\left[G\left(\frac{\partial d_1}{\partial y} + \frac{\partial d_2}{\partial x}\right)\right] = F_1 \quad (16)$$

$$\rho_w\frac{d^2 d_2}{dt^2} - \frac{\partial}{\partial x}\left[G\left(\frac{\partial d_1}{\partial y} + \frac{\partial d_2}{\partial x}\right)\right] - \frac{\partial}{\partial y}\left[(\lambda+2G)\frac{\partial d_2}{\partial y} + \lambda\frac{\partial d_1}{\partial x}\right] = F_2 \quad (17)$$

Neglecting centrifugal force or gravitational force, F_1 and F_2 shown in equations (16-17) are with a value of zero. To close the above differential system, boundary conditions need to be specified on the entire boundary. At two ends of the elastic material, we specify $\frac{dd_i}{dx_i} = 0$, where i = 1, 2. On the vessel wall, we specify force-type boundary conditions. On physical grounds, it is required that stresses be continuous across the boundary separating the incompressible fluid flow and elastic medium. This dictates that the elastic stress, $\tau_{ij}(= \lambda\delta_{ij}d_{k,k} + G(d_{i,j} + d_{j,i}))$, be equal to the flow stress governed by Stokes' constitutive relation for stress in a Newtonian fluid, $\tau_{ij} = -p\delta_{ij}d_{k,k} + \mu(u_{i,j} + u_{j,i})$. Continuity of stresses between a fluid and an elastic material demands that

$$(\lambda + 2G)\frac{\partial d_1}{\partial x} + \lambda \frac{\partial d_2}{\partial y} = \sigma_{xx}, \quad (18)$$

$$\lambda \frac{\partial d_1}{\partial x} + (\lambda + 2G)\frac{\partial d_2}{\partial y} = \sigma_{yy}, \quad (19)$$

$$G\left(\frac{\partial d_1}{\partial x} + \frac{\partial d_2}{\partial y}\right) = \sigma_{xy}. \quad (20)$$

By definition, σ_{xx}, σ_{yy} and σ_{xy} are as follows:

$$\sigma_{xx} = -p + 2\mu\frac{\partial u}{\partial x}, \quad (21)$$

$$\sigma_{yy} = -p + 2\mu\frac{\partial u}{\partial y}, \quad (22)$$

$$\sigma_{xy} = \mu\left(\frac{\partial u}{\partial x} + \frac{\partial u}{\partial y}\right) \quad (23)$$

On the boundary separating ambient, which is naturally inviscid, and the elastic vessel, we assume that $p = 0$. As a result, it is rational to prescribe $\sigma_{xx} = \sigma_{yy} = \sigma_{xy} = 0$. The advantage of applying the finite element method to simulate the flow/structure interaction problem is apparent since the boundary force can be directly incorporated into the formulation through integration by parts.

The Navier-Stokes equations, subject to continuity equations, for modeling the flow motion are solved iteratively by using Navier equations to obtain the vessel displacement. In a specified domain, the flow equations are solved. This is followed by integrating the pressure and the shear stresses along the vessel wall to obtain the boundary force. The displacement can then be obtained by solving the Navier equations for the incompressible elastic medium. The vessel configuration is, therefore, updated, thus enabling us to solve the flow equations. This iterative procedure is repeated until the vessel shows negligible change in configuration.

三、Finite Element Analysis In Moving Grids

The finite element method has been accepted as an effective tool for tackling complex geometries and implementing Neumann-type boundary conditions. These attributes motivated us to use this method to simulate flow in a compliant vessel. For describing the proposed finite element model, we will first consider the transport equation (8) and discretize it using a semi-discretization finite element model. Following the standard procedures, we can derive the corresponding ordinary differential equation on bi-quadratic elements as follows:

$$\underline{\underline{B}}\left.\frac{d\underline{\phi}_j}{dt}\right|_{(\tau,t)} + \underline{\underline{A}}\,\underline{\phi}_j = \underline{S} \quad (24)$$

We then approximate the remaining temporal derivative $\frac{d\phi}{dt}$ using the second-order accurate forward time-stepping scheme ($\left.\frac{d\phi}{dt}\right|_j = \frac{1}{2\Delta t}\left(3\phi_j^{n+2} - 4\phi_j^{n+1} + \phi_j^n\right)$). The resulting algebraic system reads as

$$\frac{3}{2\Delta t}\underline{\underline{B}}\phi_j^{n+2}\Big|_{(\tau,t)} = \underline{S} + \left(\frac{2}{\Delta t}\underline{\underline{B}} - \underline{\underline{A}}\right)\phi_j^{n+1}\Big|_{(\tau,t)} - \frac{1}{2\Delta t}\underline{\underline{B}}\phi_j^n\Big|_{(\tau,t)} \quad (25)$$

The above Galerkin approximation provides solutions which are formally second-order accurate in space as well as in time for cases with uniform grid size.

The solution to equations (9-11) can be obtained using the mixed finite element matrix equation, which contains as many diagonal zeros as does the continuity equation. The pressure appearing only in the momentum equations makes it difficult to calculate field variables from the matrix equations. We denote the constrained space $L_0^2(\Omega)$ for the pressure. In the present mixed finite element formulation, we introduce the Sobolev space $H_0^1(\Omega)$ for the velocity vector. Solutions are then sought for $\underline{u} \in H_0^1(\Omega)$ and $p \in L_0^2(\Omega)$ from the weak statement for equations (9-11). In this Galerkin finite element analysis, the test functions $\underline{w} \in H_0^1(\Omega) \times H_0^1(\Omega)$ and $q \in L_0^2(\Omega)$ are used for the vector and scalar quantities, respectively. To get rid of the undesired pressure mode, we employ biquadratic polynomials, N_i, to approximate $\underline{u}$ and the

bilinear polynomials, M_i, to approximate p since this variable setting accommodates the inf-sup (or div-stability) condition (Brezzi & Douglas (1988), Babuska (1973) and Brezzi (1974)). The resulting ordinary equation can, as before, be discretized using the above-mentioned second-order time-stepping scheme.

四、Verification Of The Finite Element Models

As a first step towards verifying the finite element model developed for simulation of fluid flows on moving grids, we have successfully solved the variable transport equation, which is amenable to analytical solution. For completeness, theoretical verification of the Navier-Stokes code is also provided. The reader is referred to (Sheu & Chen 1999) for additional details.

In the following, we will justify the finite element model developed to solve the linear elastic equations for obtaining the time-varying displacement vector. Given the force vector $\underline{F} = e^{-t}((x^2 y^2 - 6y^2 - 8xy - 2x^2), (x^2 y^2 - 6x^2 - 8xy - 2y^2))$, equations (16-17) were solved subject to analytical boundary conditions. To start the calculation at $t = 0$, we uniformly discretized the domain in $0 \le x, y \le 1$, resulting in a grid system with a resolution of 11 X 11. Calculation terminated at $t = 2$ with a uniform time increment $\Delta t = 10^{-3}$. We will consider the case with $\rho_w = G = a = 1$. Under these circumstances, the exact displacement vector has the same solution as the specified velocity vector $\underline{u} = e^{-t} x^2 y^2 (-1, -1)$. The prediction errors are cast in their L_2-norm for displacements. As Table 1 shows, the present finite element code can be applied with confidence to analyze linear elastic equations.

We also validated the finite element code developed to simulate elastic equations in cylindrical coordinates. The material properties remained the same as those considered in the Cartesian coordinates. Subject to the boundary conditions, the exact displacements were derived as $d_1 = d_2 = e^{-t} x^2 y^2$ on the condition that the force vector shown in equations (16-17) was specified as $(F_1, F_2) = (e^{-t}(x^2 y^2 - 6y^2 - 12xy - 4x^2), e^{-t}(x^2 y^2 - 9x^2 - 8xy - 2y^2))$. The unit square domain $0 \le x, r \le 1$ was uniformly discretized to a 11 X 11 mesh. The computed L_2- error norms, tabulated in Table 2, demonstrated the validity of the employed temporally and spatially second-order accurate finite element formulation for solving the elastic equations. This was followed by verification of the finite element code used to solve elastic equations in cylindrical coordinates. The problem studied previously by Xu and Collins (Xu & Collins 1995) is that of a tube with a wall thickness of 1 *mm*, an inner diameter of 10 *mm* and an outer diameter of 12 *mm*. In the following calculation, we considered that the tube had a Young's modulus of 5 X 10^5 *Pa*, a density of 10^3 *kg/m*^{3} and a Poisson ratio of 0.49.

To simplify the analysis so that the elastic equations in cylindrical coordinates were amenable to exact solutions, we assumed that the tube was long enough to rationally avoid specifying axial boundary conditions. Under these circumstances, the thick-walled tube displacement in the radial direction could be analytically determined under a uniform pressure $\bar{p}$ = 2688 *Pa* according to the following equation (Love 1952):

$$d_r = \frac{r_i \bar{p}}{r(r_o^2 - r_i^2)E}\left[(1+\bar{\nu})r_o^2 + (1-\bar{\nu})r^2\right] \quad (26)$$

In the above, r_i and r_o denote the inner and outer diameter of the tube. As for the material properties $\bar{\nu}$ and E, they are, respectively, known as the Young's modulus and Poisson ratio.

Based on the specified values of r_i, r_o, E, $\bar{\nu}$, and $\bar{p}$, we performed finite element calculations in a domain discretized by 11 X 201 mesh points. To justify the prediction, we plot the radial displacement d_r against r in Fig. 1 it is seen that finite element solutions agree perfectly with the exact solution (symbol) of equation (27). According to the computed and analytic solutions tabulated in Table 3, the computed L_2 - error norm is $0.2736216\ 10^{-9}$.

五、Computed Results

Having obtained the excellent agreement between the model predictions and all of the analytic solutions, we will now explore more complex flow phenomena in a channel with a moving indentation. This problem, schematically shown in Fig. 2, has been experimentally studied by Pedley and Stephanoff (1985), and numerically simulated by Ralph and Pedley (1988), Demirdzic and Peric (1990), and Rosenfield et al. (1991). The channel wall is rigid everywhere except at the indentation, which is placed downstream of the channel inlet. The indentation, made of a thick and stiff rubber membrane, changes its shape owing to a piston moving upwards and downwards, with a maximum indentation movement of 0.38 measured from the upper wall of the channel.

The configuration of the indented wall is algebraically represented by

$$y(x) = \begin{cases} 0.19h\left(1-\cos\left(\frac{2\pi t}{T}\right)\right) & ;0 \le x \le x_1 \\ 0.085h\left(1-\cos\left(\frac{2\pi t}{T}\right)\right)\left(1-\tanh\left(a(x-x_2)\right)\right) & ;x_2 \le x \le x_3 \\ 0 & ;x > x_3 \end{cases} \quad (27)$$

In the above, h and T denote the channel height and the oscillation period. Free parameters intended for use to define the time-varying indented wall are chosen as a = 4.14, $x_1 = 4h$, $x_2 = 5.25h$, and $x_3 = 6.5h$.

As in many simulations of inflow-outflow problems, the outlet is truncated far downstream of the indentation. he length is chosen to be 40 to save disk storage and, us, computing time. At the inlet, velocity profile of the fully-developed type is specified while the outlet low is assumed to be fully-developed again with vanishing values of ν and $\frac{\partial u}{\partial x}$. At t = 0, the initial flow condition is obtained under the fully-developed condition without considering the indentation movement. The flow under investigation has a Reynolds number Re = 100 and a Strouhal number $St = \frac{hf}{\bar{U}}$ = 0.03, where f denotes the oscillating frequency of the moving piston. The Reynolds number considered in this case is defined by choosing the channel height h as the referenced length and the averaged entrance velocity $\bar{U}$ as the characteristic velocity. The computational grid used for the present analysis has 21 X 551 points, which are non-uniformly distributed in the channel. To resolve time-evolving flow details, grids are clustered near the channel wall and in regions downstream of the indentation. At each time, the boundary grids are generated according to the specified moving indentation while the interior grids are re-distributed according to the computed grid velocities.

To give a global picture of the flow development in the channel with a moving indentation, we plot first the instantaneous streamlines at ten chosen dimensionless times, starting from t=0.2 to t=1.1 with a time increment Δt = 0.1 . As Fig. 3 shows, immediately downstream of the indentation the flow field is configured with a single eddy, in the early flow development stage. As time goes by, a second separated eddy forms on the opposite side of the channel. Later on, another smaller and weaker eddy forms on the channel floor. Such a vortex-shedding-like flow feature, considered as a manifestation of the entire flow development, is reproduced as that obtained experimentally by Pedley and Stephanoff (1985), and numerically by of Ralph and Pedley (1988) and Rosenfield et al. (1991). The time-evolving vortex shedding phenomenon can be seen also in the pressure contours shown in Fig. 4.

In order to demonstrate the applicability of the present flow/structure finite element model, we have performed numerical simulation of a problem previously analyzed by Xu and Collins (1995). The coupled fluid/solid problem involves an incompressible fluid flow in an elastic tube of finite length. The tube with a length of 5 *cm* and a thickness of 1 *mm* has inner and outer diameters of 10 *mm* and 12 *mm*, respectively. In this simulation, two ends of the cylindrical elastic tube were fixed. We divided the linearly elastic tube into 7 fluid

elements and 2 solid elements in each radial direction. The two media in the axial direction were discretized by 20 elements. At the vessel inlet, we specified that the pressure be harmonically changed according to $\frac{\partial p}{\partial x} = -Ae^{\text{int}}$, where A is an arbitrary constant. This problem had been studied by Xu and Collins (1995) and was chosen here to study the coupled fluid/solid motion mainly because this problem is amenable to an analytical solution (Womersley 1957). Given the initial conditions, we had iteratively analyzed the coupled fluid/solid problem since the wall position at the updated time level was unknown. Within each time step, we estimated the position of the vessel based on the currently available grid velocities. This is followed by carrying out the incompressible flow calculations to obtain pressures that are applied on the mostly updated domain boundary. We then solved for the linearly elastic equations to obtain the new vessel configuration. Having obtained the updated physical domain, we proceeded to solve the flow equations. The above iterative procedure was repeated until the specified tolerances on the vessel displacements were obtained. Following the above coupled fluid/solid solution procedure, we could obtain finite element solutions for the axial velocity. As Fig. 5 shows, which plots the axial velocity $U_x(r)$ at four arbitrarily chosen times, good agreement between the prediction and the analytical data given below was obtained (Womersley 1957) :

$$u_x = \frac{A}{\circ}\frac{1}{in}\left\{1 + {}' \frac{J_0\left(\sim y i^{3/2}\right)}{J_0\left(\sim i^{3/2}\right)}\right\} int \quad (28)$$

六、Condluding Remarks

In this paper, a Galerkin finite element model has been presented forthe prediction of flow in a domain bounded partly by an elastic moving boundary. To facilitate the analysis, working equations have been derived in moving coordinates so as to adapt to the flow. It is noteworthy that satisfaction of the geometric conservation law property is essential for analyses conducted on moving grids. In the spatial discretization, we applied the Galerkin finite element method to obtain a second-order spatially accurate solution. The remaining ordinary differential equation, which involves time derivatives, was discretized using the second-order accurate time-stepping method. The proposed model for fluid flow equations in moving grids has been theoretically verified. In addition, the finite element model developed to solve Navier equations for elastic media has been analytically verified. Results have also been presented for the flow in a vessel, where part of its rigid/elastic surface bounding the physical flow region moves in time.

五、參考文獻

[1] BREZZI F. (1974), On the existence, uniqueness and approximation of saddle point problem analysis from Lagrangian multipliers. RAIRO, Anal. Num. 8(R2) 129-151.

[2] BABUSKA, I. (1973), The finite element method with Lagrangian multipliers Numer. Math., {\bf 20}, 179-192.

[3] D EMIRDIZIC I. and PERIC M. (1990), Finite volume method for prediction of fluid flow in arbitrarily shaped domains with moving boundaries. Int. J. Numer. Meths. Fluids, 10, 771-790.

[4] DEMIRDIZIC I. and P ERIC M. (1983), Space conservation law in finite volume calculation of fluid flow. Int. J. Numer. Meths. Fluids, bf 8, 1037-1050.

[5] DEMIRDIZIC I. and PERIC M. (1983), Space conservation law in finite volume calculation of fluid flow. Int. J. Numer. Meths. Fluids, 8, 1037-1050.

[6] KU D. N., GIDDENS D. P., ZARINS C. K., GLAGOV S. (1985) Pulsatile flow and atherosclerosis in the human carotid bifurcation : postive correlation between plaque location and low and oscillatory shear stress. Arteriosclerosis, 5, 293-302.

[7] LADYZHENSKAYA O. (1969), The Mathematical Theory of Viscous Incompressible Flow. Gordon and Breach, New York.

[8] LOVE, A. E. H. (1952), A Treatise on the Mathematical Theory of Elasticity. Cambridge University Press.

[9] ROSENFIELD, M., KWAK, D., and VINOKUR M. (1991), A fractional step solution method for

the unsteady incompressible Navier-Stokes equations in generalized coordinate systems. J. Comp. Phys., 94(1), 102-137.

[10] RALPH M. E. and PEDLEY T. J. (1988), Flow in a channel with a moving indentation. J. Fluid Mech., 190, 87-112.

[11] OGAWA SATORU and ISHIGURO TOMIKO (1987), A method for computing flow fields around moving bodies. J. Comput. Phys., 69, 49-68.

[12] SCHOUTEN J. A. (1954), An Introduction to Tensor Analysis and its Geometrical Applications. Ricci-Calculus, Springer-Verlag, Berlin.

[13] SHEU, W. H., CHEN Y. H. (1999), A transient analysis of incompressible fluid flow in vessels with moving boundaries. Int. J. Numer. Meths. Heat & Fluid Flow, 9(8), 833-846.

[14] PEDLEY, T. J. and STEPHANOFF K. D. (1985), Flow along a channel with a time-dependent indentation in one wall : The generation of vorticity waves. J. Fluid Mech., 160, 337-367.

[15] THOMAS P. D., LOMBARD C. K. (1979), Geometric conservation law and its application to flow computations on moving grids. AIAA J., {\bf 17(10)}, 1030-1037.

[16] TRULIO J. G. and TRIGGER K. R. (1961), Numerical Solution of the One-dimensional Hydrodynamic Equations in an Arbitrary Time-dependent Coordinate System. University of California Lawrence Radiation Laboratory Report UCLR-6522.

[17] WOMERSLEY, J. R. (1957), The Mathematical Analysis of the Arterial Circulation in a State of Oscillatory Motion. WADC-TR56-614, Wright Air Development Center.

[18] XU, Y. Y., COLLINS, M. W. (1995), Numerical modelling of blood flow in compliant arteries and arterial bifurcations. Bio-fluid Mechanics, editor H. Power, Computational Mechanics Publications, Southampton Boston, 55-93.

Time	d_1 L_2-norm	d_2 L_2-norm
0.5	0.7693×10^{-8}	0.1298×10^{-8}
1.0	0.1113×10^{-8}	0.6656×10^{-8}
1.5	0.1335×10^{-8}	0.2987×10^{-8}
2.0	0.1129×10^{-8}	0.9524×10^{-8}

Table 1. The computed L_2-error norms for displacements governed by elastic equations (16-17).

Time	d_1 L_2-norm	d_2 L_2-norm
0.5	0.7693×10^{-8}	0.1298×10^{-8}
1.0	0.1113×10^{-8}	0.6628×10^{-8}
1.5	0.1335×10^{-8}	0.2987×10^{-8}
2.0	0.1129×10^{-8}	0.9524×10^{-8}

Table 2. The computed L_2-error norms for displacements governed by elastic equations cast in cylindrical coordinates.

r position	exact	numberical
5 mm	0.1610×10^{-3}	0.1610×10^{-3}
5.2 mm	0.1572×10^{-3}	0.1572×10^{-3}
5.4 mm	0.1538×10^{-3}	0.1538×10^{-3}
5.6 mm	0.1507×10^{-3}	0.1507×10^{-3}
5.8 mm	0.1480×10^{-3}	0.1480×10^{-3}
6.0 mm	0.1455×10^{-3}	0.1455×10^{-3}

Table 3. A comparison of computed and analytical solutions computed at six chosen radial locations.

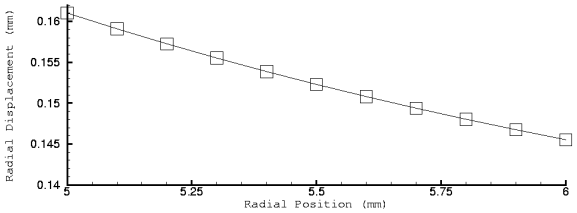

Figure 1. The computed radial displacements d_r. The exact solutions are represented by the symbols in the figure.

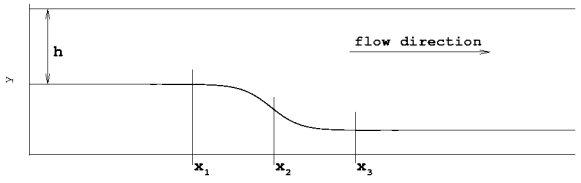

Figure 2. Schematic of the indented wall.

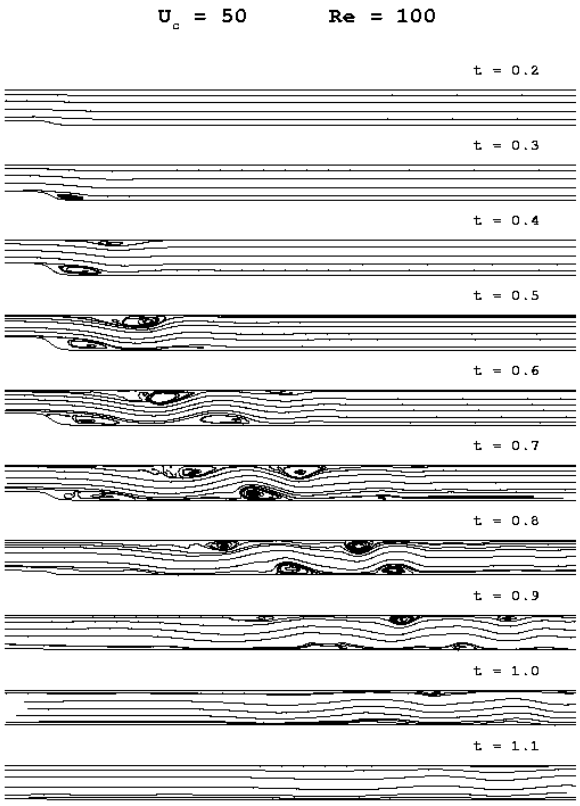

Figure 3. The computed time-varying streamlines.

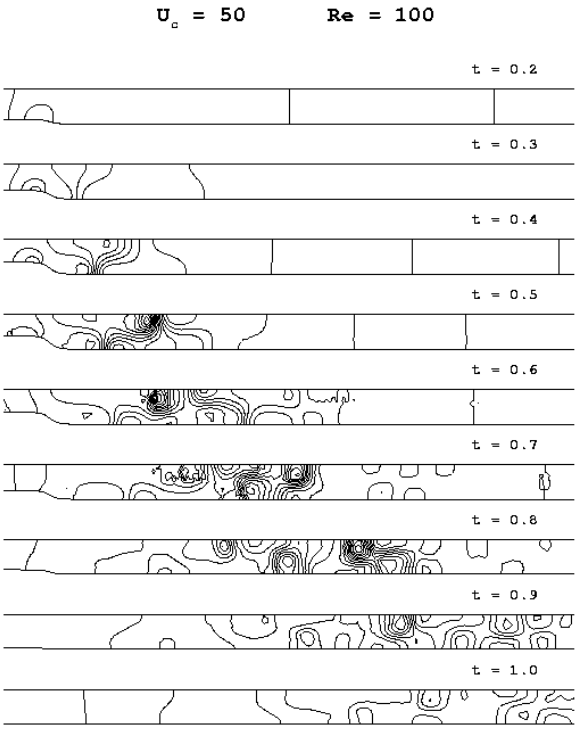

Figure 4. The computed time-varying pressure contours.

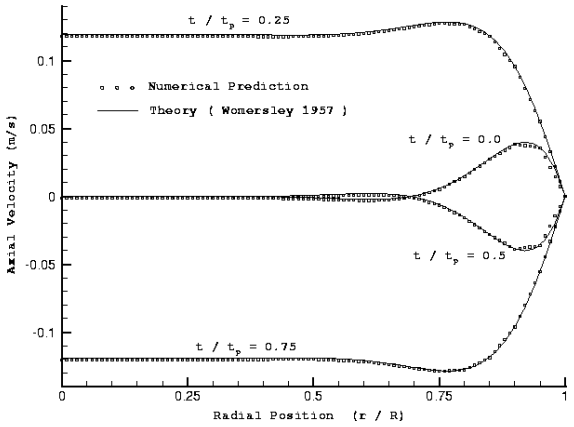

Figure 5. Analytical and predicted axial velocity profiles for transient flow in a compliant tube.